Geophysical Journal International

Geophys. J. Int. (2017) **209,** 1326–1336
Advance Access publication 2017 March 1
GJI Geomagnetism, rock magnetism and palaeomagnetism

doi: 10.1093/gji/ggx088

Generation of MAC waves by convection in Earth's core

Etienne Jaupart[1] and Bruce Buffett[2]

[1]*Department of Physics, Ecole Normale Superieure de Lyon, Lyon Cedex* 07*, France*
[2]*Department of Earth and Planetary Sciences, University of California, Berkeley, CA* 94720*, USA. E-mail: bbuffett@berkeley.edu*

Accepted 2017 February 28. Received 2017 February 22; in original form 2016 October 30

SUMMARY

Convection in Earth's core is a viable mechanism for generating MAC waves when the top of the core is stably stratified. We quantify the generation mechanism by extending the physical description of MAC waves to include a source term due to buoyancy forces in the convecting part of the core. Solutions for the forced motion are obtained using a Green's function, which is constructed from the eigenfunctions for the unforced motion. When the source term is evaluated using the output of a numerical geodynamo model, the largest excitation occurs at even spherical harmonic degrees, corresponding to waves with symmetric azimuthal flow about the equator. We also find that the magnitude of the source term decreases at periods shorter than about 60 yr. As a result most of the wave generation is confined to waves with periods of 60 yr or longer. Quantitative predictions for the wave amplitudes depend on the projection of the source term into the eigenfunction of the waves. Strong stratification limits the penetration of density anomalies into the stratified layer, which means that the source term is confined to the lowermost part of the layer. Overtones of MAC waves with large amplitudes in the lower part of the stratified layer are more effectively generated by convection, even though these waves are heavily damped by magnetic diffusion. Generation of MAC waves by convection establishes a physical link between observable wave motion and deeper convective processes. Detection of changes in the amplitude and phase of MAC waves would constrain the generation processes and offer insights into the nature of the convection.

Key words: Composition and structure of the core; Geomagnetic induction; Rapid time variations.

1 INTRODUCTION

Stable stratification in Earth's core permits long-period waves with a primary force balance between magnetic, Archimedes and Coriolis forces (sometimes called a MAC balance). Inertia has little influence on the wave motion, so the time dependence is due to changes in the local magnetic field and disturbances in the density stratification. Buoyancy and Lorentz forces are the main restoring forces for the waves, and representative estimates yield periods of several decades (Braginsky 1993). Evidence for zonal waves in the core has been reported on the basis of two models for core-surface flow (Jackson 1997; Wardinski & Lesur 2012). Predictions for fluctuations in the dipole field (Buffett 2014) were found to be in good agreement with observations (Jackson *et al.* 2000; Gillet *et al.* 2013). Subsequent investigations using a third model for core-surface flow (Gillet *et al.* 2015) produced consistent results for the strength and thickness of fluid stratification (Buffett *et al.* 2016).

Damping of MAC waves by ohmic dissipation requires continual excitation to sustain the waves over time. Convection in the interior of the core is a likely source of excitation. Buoyant fluid rises toward the stratified layer at the top of the core, disturbing the density stratification and initiating wave motion. Turbulent convection in the Sun has a similar role in generating internal waves in the stably stratified radiative zone (Press 1981; Lecoanet & Quataert 2012). However, there are important distinctions due to the style of convection. Convection in the Sun produces strong inertial effects, which contribute significantly to the generation of internal waves (e.g. Press 1981). By comparison, inertial forces in the core are thought to be many orders of magnitude smaller than the leading-order forces. For example, a nominal estimate for the ratio of inertia to Coriolis forces in the core is roughly 10^{-6} (Aurnou *et al.* 2015). Thus, buoyancy forces due to temperature or compositional anomalies should be important for generating MAC waves. Reynolds stresses are sometimes invoked to explain the generation of torsional waves (Teed *et al.* 2014), although magnetic stresses should have a larger role at Earth-like conditions (Teed *et al.* 2015). Buoyancy forces are not effective in generating torsional waves because the wave motion is perpendicular to the direction of gravity (Braginsky 1984).

A description of wave generation by turbulent motion was initially formulated in the context of acoustic waves (Lighthill 1952). This general approach was later extended to include internal waves (Stein 1967; Phillips 1966). Subsequent studies have applied this

approach to a wide range of problems (Goldreich & Kumar 1990; Houdek *et al.* 1999; Pandya & Alexander 1999; Lecoanet *et al.* 2015). We extend these applications by investigating the problem of MAC wave generation due to convection in the core. We develop a description of the MAC waves that includes various source terms, including contributions from buoyancy, inertial and magnetic forces. Solutions for the forced motion are sought using a Green's function, which can be constructed from the eigenfunctions of the wave problem.

Estimates for the source terms are evaluated using a numerical dynamo model. We focus on a numerical model that includes a thermally stratified region at the top boundary to capture the influences of a thin non-convecting region on the generation process. Insights are drawn from the temporal and spatial dependence of the source term, particularly concerning the symmetry of the wave generation. We also gain insights into the prominence of overtones that were reported in Buffett *et al.* (2016). Even though the higher overtones are more heavily damped, their presence in the observations can be explained by the nature of the excitation. Finally, we speculate about the possibility of using observations of the waves to draw conclusions about convection deep inside the core.

2 DESCRIPTION OF MAC WAVES

We consider the evolution of small perturbations in density, ρ', velocity, $\mathbf{v}$, and magnetic field, $\mathbf{b}$, in a thin layer at the top of the core. These perturbations are superimposed on background fields, $\bar{\rho}$, $\mathbf{V}$ and $\mathbf{B}$, which are taken to be steady over the period of the waves. The shallow depth of the layer compared with its horizontal extent permits several standard approximations. We can assume that the radial gradient in the perturbations is large compared with the horizontal gradients or with the gradients in the background fields. We can also retain only the radial component of the rotation vector in the Coriolis force (e.g. Pedlosky 1987). Following Braginsky (1993) we adopt a Boussinesq approximation and assume inviscid flow. With these approximations the linearized equations for $\mathbf{v}$ and $\mathbf{b}$ are

$$\partial_t \mathbf{v} + \mathbf{V}\cdot\nabla\mathbf{v} + 2\boldsymbol{\Omega}\times\mathbf{v} = -\frac{1}{\bar{\rho}}\nabla P + \frac{1}{\bar{\rho}\mu}B_r\partial_r\mathbf{b} + c\mathbf{g} \tag{1}$$

$$\partial_t \mathbf{b} = B_r\partial_r\mathbf{v} + \eta\nabla^2\mathbf{b} \tag{2}$$

$$\nabla\cdot\mathbf{v} = \nabla\cdot\mathbf{b} = 0 \tag{3}$$

where $\boldsymbol{\Omega}$ includes only the radial part of rotation vector, μ is the magnetic permeability, $c = \rho'/\bar{\rho}$ is the relative density perturbation, $\mathbf{g} = -g\hat{\mathbf{r}}$ is the acceleration due to gravity, and $\eta = (\mu\sigma)^{-1}$ is the magnetic diffusivity. Here σ is the electrical conductivity of the core.

Perturbations in density (and hence changes in c) can arise in two ways. They can occur by radial motion through the stable density gradient (nominally $\partial\bar{\rho}/\partial r$). Alternatively, they can occur when density perturbations are swept into the stratified layer by the underlying convection. In an incompressible fluid

$$\frac{D\rho'}{Dt} = \frac{\partial\rho'}{\partial t} + \mathbf{V}\cdot\nabla\rho' + \mathbf{v}\cdot\nabla\bar{\rho} = 0 \tag{4}$$

so the buoyancy force in (1) evolves according to

$$g\frac{\partial c}{\partial t} = N^2\mathbf{v}\cdot\hat{\mathbf{r}} - g\mathbf{V}\cdot\nabla c \tag{5}$$

where

$$N^2 = -\frac{g}{\bar{\rho}}\frac{\partial\bar{\rho}}{\partial r} \tag{6}$$

is the squared buoyancy frequency. The first term on the right-hand side of (5) represent the change in buoyancy force due to stable stratification. The second term represents the effect of density anomalies due to convection in the core. The latter is treated as a source term for the waves. Omitting the source term defines the unforced motion, which specifies the frequency and spatial structure of the waves. The forced motion is evaluated using a Green's function.

3 SOLUTION FOR ZONAL MAC WAVES

Braginsky (1993) obtained analytical solutions for zonal waves when the effects of local inertia were omitted from the momentum equation in (1). This approximation is reasonable because the wave period is much longer than the rotation period. He also restricted $\mathbf{B}$ to a dipole field to obtain solutions by separation of variables in spherical coordinates (r, θ, ϕ). We adopt the same approximation here, even though the spatial structure of the waves is altered by the presence of radial magnetic field in the equatorial region. Any change in the waves is liable to affect their excitation, but the general methodology outlined here does not dependent on these details. We simply use the analytical solutions of Braginsky (1993) as an illustrative example.

The governing equations in Section 2 can be reduced to a single, scalar wave equation for the azimuthal component of the magnetic field perturbation (i.e. b_ϕ). The steps leading to the scalar wave equation are described in Braginsky (1993), so we include only a few details in Appendix A. The resulting wave equation can be written in the form

$$\partial_t^2 b_\phi(r,\theta,t) - \eta\partial_r^2\partial_t b_\phi(r,\theta,t) - \left(\frac{V_a N}{2\Omega R}\right)^2 \mathcal{L}_\theta^2\, b_\phi(r,\theta,t) = S \tag{7}$$

where the source term due to buoyancy fluctuations is

$$S = \frac{gB_d}{2\Omega R}\,\partial_\theta(\mathbf{V}\cdot\nabla c) \tag{8}$$

and the operator $\mathcal{L}_\theta^2$ is defined by

$$\mathcal{L}_\theta^2(\cdot) \equiv \partial_\theta\left(\frac{1}{\sin\theta}\partial_\theta\{\sin\theta\,(\cdot)\}\right). \tag{9}$$

We use B_d to define the amplitude of the dipole ($B_r = B_d\cos\theta$) and introduce

$$V_a = \frac{B_d}{\sqrt{\rho\mu}} \tag{10}$$

to characterize the magnetic part of the restoring force. (V_a represents an Alfven velocity for the radial magnetic field). Similarly, we use Ω to denote the amplitude of the rotation vector ($\Omega_r = \Omega\cos\theta$) and let R be the radius of the core–mantle boundary (CMB). It is clear from (7) that the waves depend on the radial magnetic field (through V_a) and the density stratification (through N). Damping of the waves occurs by magnetic diffusion, which is represented by the second term on the left-hand side of (7).

The wave problem is defined by setting $S = 0$. Introducing the Fourier transform, defined by

$$\tilde{b}_\phi(r,\theta,\omega) = \int_{-\infty}^{\infty} b_\phi(r,\theta,t)e^{i\omega t}\,\mathrm{d}t\,, \tag{11}$$

we convert the wave equation in (7) to the frequency domain

$$-\omega^2\tilde{b}_\phi(r,\theta,\omega) + i\omega\eta\partial_r^2\tilde{b}_\phi(r,\theta,\omega) - \left(\frac{V_a N}{2\Omega R}\right)^2 \mathcal{L}_\theta^2\,\tilde{b}_\phi(r,\theta,\omega) = 0 \tag{12}$$

where ω is the frequency of the wave motion. Because the variables r and θ are separable, solutions can be found in the form

$$\tilde{b}_\phi(r,\theta,\omega) = \tilde{b}_l(r,\omega)P_l^1(\cos\theta) \tag{13}$$

where $P_l^1(\cos\theta)$ is the associated Legendre function with $m = 1$. Noting that

$$\mathcal{L}_\theta^2 P_l^1(\cos\theta) = -l(l+1)P_l^1(\cos\theta) \tag{14}$$

the wave equation reduces to

$$-\omega^2\tilde{b}_l(r,\omega) + i\omega\eta\,\partial_r^2\tilde{b}_l(r,\omega) + \omega_l^2\tilde{b}_l(r,\omega) = 0 \tag{15}$$

where

$$\omega_l = \sqrt{l(l+1)}\left(\frac{V_a N}{2\Omega R}\right) \tag{16}$$

defines the restoring force for waves with degree l.

Solutions to the wave equation in (15) are subject to boundary conditions at the top and bottom of the stratified layer. At the CMB ($r = R$) we impose insulating conditions on the toroidal component of the magnetic field (Braginsky 1993)

$$\tilde{b}_l(R,\omega) = 0\,. \tag{17}$$

We also impose continuity conditions on $b_l(r,\omega)$ and $\partial_r b_l(r,\omega)$ at the base of the stratified layer ($r = R - H$), where H is the layer thickness. The solution inside the layer is matched to a solution below the stratified layer, where $\omega_l = 0$. Setting $\omega_l = 0$ in (15) defines a diffusion equation, which corresponds to a standard skin-depth problem (Gubbins & Roberts 1987). This solution allows the magnetic field at the base of the stratified layer to decay to zero in the interior of the core over a distance

$$\delta = \sqrt{\frac{2\eta}{\omega}}\,. \tag{18}$$

For representative frequencies, the skin depth is small compared to H, so the solution for $\tilde{b}_l(r,\omega)$ is mainly confined to the stratified layer and its immediate vicinity. Braginsky (1993) found solutions for $\tilde{b}_l(r,\omega)$ in terms of a stretched coordinate $x = (R - r)/H$. His solutions were expressed in the form

$$\tilde{b}_l(x,\omega) = \tilde{b}_l(\omega)\sin(\alpha x) \tag{19}$$

where α is a constant. When δ/H is vanishingly small $\alpha \approx \pi$ and $\omega \approx \omega_l$. Leading-order corrections for finite values of δ/H are

$$\alpha \approx \pi\left(1 - \frac{\delta}{2H}(1+i)\right) \tag{20}$$

and

$$\omega \approx \omega_l\left(1 - i\frac{\pi^2\delta^2}{4H^2}\right)\,. \tag{21}$$

We can also find solutions with larger radial wavenumbers, $\alpha \approx n\pi$, for $n = 2, 3, \ldots$, although these overtones are more heavily damped. We now use these solutions to estimate the forced response due to convection in the interior of the core.

4 GENERATION OF WAVES BY BUOYANCY FORCES

The source term for wave motion in (8) defines the rate of change of fluid density in the vicinity of the stratified layer. We confine our attention to zonal waves, so we represent the density fluctuations in the form

$$\mathbf{V}\cdot\nabla c = \sum_{l=1}^{\infty} s_l(r,t)P_l^0(\cos\theta)\,. \tag{22}$$

where s_l is the amplitude of zonal density fluctuations at degree l. Substituting (22) into (8) yields

$$S(r,\theta,t) = -\frac{gB_d}{2\Omega R}\sum_{l=1}^{\infty} s_l(r,t)P_l^1(\cos\theta) \tag{23}$$

where we have used the relation $\partial_\theta P_l^0(\cos\theta) = -P_l^1(\cos\theta)$. We now exploit the orthogonality of the Legendre functions to decompose the forced problem into a set of independent equations for each degree l. Introducing $S(r,\theta,t)$ into the Fourier transform of the general wave equation in (7) and using the solution for $b_\phi(r,\theta,\omega)$ from (13) gives

$$-\omega^2\tilde{b}_l(r,\omega) + i\omega\eta\partial_r^2\tilde{b}_l(r,\omega) + \omega_l^2\tilde{b}_l(r,\omega) = -\left(\frac{gB_d}{2\Omega R}\right)\tilde{s}_l(r,\omega) \tag{24}$$

for the forced response at each l.

We proceed by constructing a Green's function for the response to an impulsive forcing. When the density fluctuation is represented by a delta function in time (i.e. $s_l(r,t) = s_l(r)\delta(t)$), the Fourier transform is simply $\tilde{s}_l(r,\omega) = s_l(r)$. Immediately after the application of an impulsive force the motion can be expressed as a linear combination of MAC waves. In other words, the solution at each degree l can be represented by

$$b_l(r,t) = \sum_k c_k\, b_l^{(k)}(r)\, e^{-i\omega_k t} \quad \text{for } t > 0 \tag{25}$$

where ω_k are the wave frequencies, $b_l^{(k)}(r)$ are the corresponding eigenfunctions and c_k are constants that depend on the excitation $s_l(r)$. Because we are dealing with the response at a particular degree l, the summation over eigenfunctions in (25) includes the fundamental mode ($k = 1$) and the various overtones ($k = 2, 3, \ldots$). The constants c_k are determined such that the description of the forced response in (24) is satisfied.

The steps needed to evaluate c_k are well established and commonly applied in normal-mode seismology (Dahlen & Tromp 1998). First, we require an orthogonality condition for the eigenfunctions $b_l^{(k)}(r)$ (or equivalently $b_l^{(k)}(x)$ in terms of the stretched coordinate x). Next, we take the Fourier transform of (25) to obtain $\tilde{b}_l(r,\omega)$ and substitute the result into the forced response in (24). Finally, we apply the orthogonality condition to (24) to isolate a single c_k in terms of $s_l(r)$. (Details are deferred to the Appendix B). When the excitation is defined in terms of x by $s_l(x,t) = s_l(x)\delta(t)$, the constants for the subsequent free motion are given by

$$c_k = -i\left(\frac{gB_d}{2\Omega R}\right)\int_0^{1^+} b_l^{(k)}(x)s_l(x)\,\mathrm{d}x \tag{26}$$

where the integral extends from the CMB ($x = 0$) to a depth slightly below the base of the stratified layer (at $x = 1$). We use the notation $x = 1^+$ to signify that the integral continues a short distance into the interior of the core. Because the eigenfunctions $b_l^{(k)}(x)$ vanish below the skin depth, we can terminate the integral just inside the interior

of the core. This result also implies that the generation of MAC waves depends on the source function $s_l(x)$ within or immediately below the stratified layer.

5 GENERATION OF WAVES BY OTHER FORCES

Buoyancy forces represent an important source of excitation, but other forces associated with convection may also contribute. Inertial forces are thought to be a primary mechanism for generating internal waves in the Sun (Goldreich & Kumar 1990), whereas magnetic forces are liable to be more important in Earth's core. Buoyancy forces have a direct role in the wave generation because these forces induce radial motion inside the stratified layer. As buoyant parcels rise through the convecting part of the core the force balance is expected to involve a combination of buoyancy, Coriolis, pressure and magnetic forces (Jones 2011). This force balance is altered once the parcels reach the base of the stratified layer. The effects of stratification oppose the parcel buoyancy, so the associated wave motion becomes part of the force balance. This is the origin of the generation mechanism due to buoyancy.

Inertial and magnetic forces are less direct because the radial components of these forces do not substantial alter the leading-order hydrostatic balance (see eq. A1). Similarly, the $\hat{\theta}$ component of the momentum equation describes a leading-order geostrophic balance between v_ϕ and the meridional pressure gradient (see eq. A2). The largest components of the inertial and magnetic forces occur in $\hat{\phi}$ direction and this is also the component of the momentum equation that is most easily disturbed by additional forces. Adding these forces to the $\hat{\phi}$ component of the momentum equation in (A3) alters v_θ, which induces radial motion through the continuity condition in (3).

We begin with the inertial force and denote the $\hat{\phi}$ component by

$$f_\phi = -(\mathbf{V}\cdot\nabla\mathbf{V})\cdot\hat{\phi}\,. \tag{27}$$

Adding f_ϕ to the right-hand side of (A3) and repeating the derivation of the wave equation for b_ϕ from Appendix A yields the (Reynolds) source term

$$S_R = \frac{B_d N}{4\Omega^2 R^2}\mathcal{L}_\theta^2\left(\frac{F_\phi}{\cos\theta}\right) \tag{28}$$

where

$$F_\phi(r,\theta) = \int_R^r f_\phi(r',\theta)\,\mathrm{d}r'\,. \tag{29}$$

The source term in (28) is singular at the equator (i.e. $\cos\theta = 0$) when F_ϕ is represented by an odd spherical harmonic degree l. This is simply a consequence of the vanishing Coriolis force at the equator, which alters the nature of the force balance and means that we cannot evaluate v_θ on the equator from (A3). A modified description of the dynamics and the source term is required at the equator, but most of the core surface is well represented by (28). For the purpose of making an order-of-magnitude estimate in the next section, we approximate the Reynolds source term by

$$S_R \approx \frac{B_d N}{4\Omega^2 R^2} l(l+1)F_\phi \tag{30}$$

where l is nominally the degree of the wave. Strictly speaking l is set by $F_\phi/\cos\theta$, which can be represented as a sum of $P_l^1(\cos\theta)$ terms with the highest degree being one less than the degree of F_ϕ (i.e. the $l = 3$ part of F_ϕ generates $l = 2$ waves). The source term due to magnetic forces is calculated in a similar way. Redefining the $\hat{\phi}$ component of the force as

$$f_\phi = -\frac{1}{\rho\mu}(\mathbf{B}\cdot\nabla\mathbf{B})\cdot\hat{\phi} \tag{31}$$

gives the approximate the (Maxwell) source term

$$S_M \approx \frac{B_d N}{4\Omega^2 R^2} l(l+1)F_\phi\,. \tag{32}$$

The strength of the stratification in (30) and (32) is evaluated in the geodynamo model using the time-averaged temperature gradient at the CMB.

6 ESTIMATE OF SOURCE TERM FROM A GEODYNAMO MODEL

The source terms can be estimated from the output of a numerical geodynamo model. We use the *Calypso* package (Matsui *et al.* 2014) and include a uniform heat sink in the temperature equation to represent the influence of conduction down the adiabatic gradient (e.g. Olson *et al.* 2015). Stable stratification develops at the top of the core when the volume-integrated heat sink exceeds the heat flow through the lower boundary (at $r = R_i$). This numerical setup approximates the effects of a sub-adiabatic heat flow at the CMB (Gubbins *et al.* 1982).

The governing equations are written in non-dimensional form using the thickness of the fluid shell $L = R - R_i$ as a characteristic lengthscale and L^2/ν as the characteristic timescale, where ν is the kinematic viscosity. Velocity is scaled by ν/L, the magnetic field is scaled by $\sqrt{\rho\mu\Omega\eta}$, and temperature is scaled by the fixed temperature difference ΔT between the top and bottom boundaries. Solutions are specified by the amplitude of the heat sink Q and by four additional dimensionless parameters:

$$E = \frac{\nu}{\Omega L^2},\quad Pr = \frac{\nu}{\kappa},\quad Pm = \frac{\nu}{\eta},\quad Ra = \frac{\alpha g(R)\Delta T L}{\nu\Omega} \tag{33}$$

which include the Ekman number, E, the Prandtl number, Pr, the magnetic Prandtl number, Pm, and a modified Rayleigh number, Ra. Here α is the coefficient of thermal expansion, $g(R)$ is the gravitational acceleration at the CMB and κ is the thermal diffusivity. Both the mantle and inner core ($r < R_i$) are assumed to be electrically insulating. An Earth-like geometry is adopted by setting $r = 1.5385$ and $r = 0.5385$ for the dimensionless radius of the core–mantle and inner-core boundaries.

An illustrative solution is obtained using $E = 5\times10^{-5}$, $Pr = 1$, $Pm = 0.5$ and $Ra = 1200$. A uniform heat source of $Q = -6$ corresponds to a (dimensionless) volume-integrated heat sink of -87.6. By comparison, the time-averaged heat flow into the base of the core is $q = -4\pi R_i^2 Pr^{-1}\mathrm{d}T/\mathrm{d}r = 69.0$. The difference drives a heat flow into the top of the core to close the energy budget. A positive radial temperature gradient develops at the CMB, producing a thin region of stable stratification (see Fig. 1). The time-averaged temperature reaches a minimum value at $r = 1.38$, so the region of stable stratification occupies the top 360 km of the core. While this thickness exceeds the value inferred in a prior study (Buffett *et al.* 2016), we avoid thinner layers in the numerical model because they have weaker stratification and less influence on the underlying convection. We prefer a layer with a discernible influence on the convection, so our model choice represents a compromise between the geometry of the layer and the strength of the stratification. Buoyant fluid rises from the inner-core boundary and penetrates into the region of stable stratification (see Fig. 2). However, many

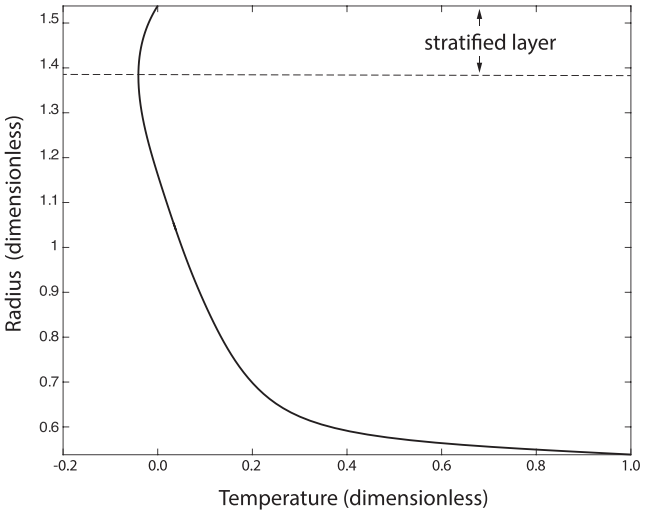

Figure 1. Time-averaged radial temperature profile from the numerical geodynamo model. A region of stable stratification develops at the top of the core when the volume-integrated heat sink in the temperature equation exceeds the heat flow across the lower boundary.

plumes are stopped by the density stratification before they reach to the top of the layer. The resulting temperature fluctuations inside and immediately below the stratified layer are responsible for exciting the MAC waves.

MAC waves are not directly detected in the dynamo model because the dimensionless parameters in the numerical calculations cause overdamped waves. Our model differs from other numerical studies that report magnetic waves in the interior of the core (Hori *et al.* 2015). MAC waves are confined to a thin layer and this short lengthscale enhances ohmic dissipation relative to waves in the interior of the core. However, we can evaluate the source terms from the numerical model. We begin with estimates for $\mathbf{V} \cdot \nabla c$ when the density anomalies are due to thermal convection (i.e. $c = -\alpha T$). Fig. 3 shows the $l = 2$ part of $-\mathbf{V} \cdot \nabla T$ as a function of time in the vicinity of the stratified layer. Positive and negative temperature fluctuations are largest below the stratified layer, although many of these fluctuations extend into the stratified zone. The largest amplitude fluctuations begin with a warming phase (positive source) as hot, buoyant parcels rise into the boundary region. The overall slope of these features reflects the radial velocity. Warming is followed by cooling (negative source) as warm parcels transit through the region and the temperature returns to the time-averaged value. All of these source terms (reflecting rates of temperature fluctuation) are subsequently multiplied by α to convert to a rate of relative density fluctuation.

The temporal dependence of the temperature fluctuations in Fig. 3 is converted to years from our dimensionless time by choosing the characteristic timescale L^2/ν. For example, a realistic value for the magnetic diffusivity, $\eta = 0.8$ m^2 s^{-1}, gives $\nu = Pm\,\eta$ or 0.4 m^2 s^{-1}. The corresponding viscous timescale, L^2/ν, is roughly 400 kyr, and the resulting root-mean-square (rms) velocity from the numerical calculation is about 0.03 mm yr^{-1}. This value is about an order of magnitude smaller than estimates inferred from core-surface flow (Holme 2015). Alternatively, we could define a timescale based on the secular variation of the magnetic field at the CMB (Hulot & Le Mouël 1994). Recent satellite field models yield a timescale of $\tau_{sv} \approx 400$ yr (Lhuillier *et al.* 2011), which can be realized in the geodynamo model when $\nu = 9.6$ m^2 s^{-1} and $L^2/\nu = 16.8$ kyr. One concern with the secular variation timescale is connected with the excess thickness of the layer in the model relative to that in the Earth. A thicker layer acts as a filter for magnetic-field variations, potentially altering the secular variation timescale in the model. Consequently, we adopt a simpler approach by defining a timescale based on the rms velocity at the core-surface. Using a value of $V_{\rm rms} = 0.38$ mm yr^{-1} from Holme (2015), we take $\nu = 5.4$ m^2 s^{-1} and $L^2/\nu = 30$ kyr to characterize the timescale of temperature fluctuations in Fig. 3. The corresponding magnetic Reynolds number, $Rm = V_{\rm rms}L/\eta$ and magnetic Ekman number, $E_\eta = E/Pm$, are 80 and 10^{-4}, respectively. These values lie outside the range recommended by Christensen *et al.* (2010) for a compliant field morphology at the CMB. The minimum recommended value for Rm at $E_\eta = 10^{-4}$ is roughly 140, as compared with 80 in our calculations. Our magnetic field is too dipolar (relative to Earth),

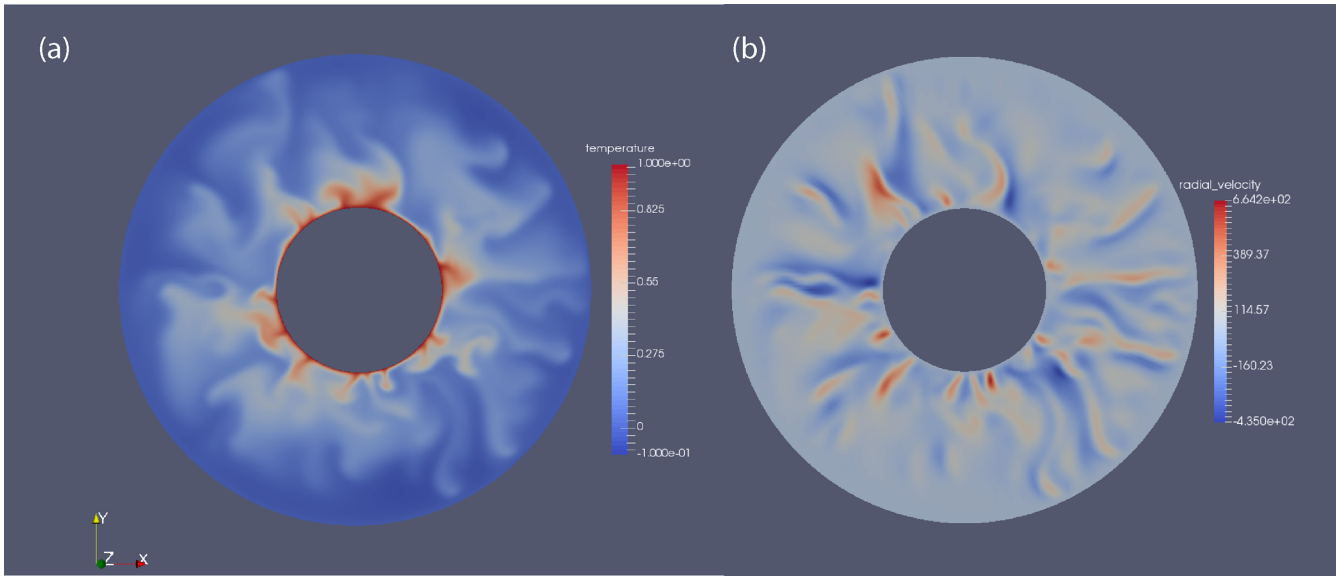

Figure 2. Snapshot of temperature (a) and radial velocity (b) in the equatorial plane from the geodynamo model. Warm plumes rise from the inner-core boundary and penetrate into the stratified layer at the top of the core. The average (inward) heat flow at the top boundary is locally reversed in locations where warm parcels reach the CMB.

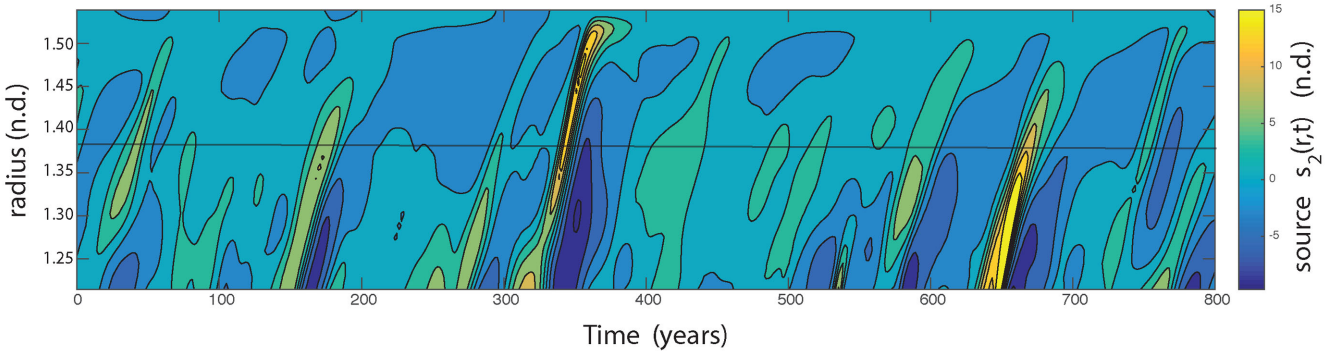

Figure 3. Source term, $s_2(r, t)$, for the degree 2 part of $-\mathbf{V} \cdot \nabla T$ in the vicinity of the stratified layer. Positive (negative) sources corresponds to warming (cooling). Short-duration warming events represent the influence of thermal plume(s) rising through the core. The slope of the source term as a function of r and t reflects the radial velocity of plumes. The recurrence time of warming events is irregular but typically exceeds 100 yr.

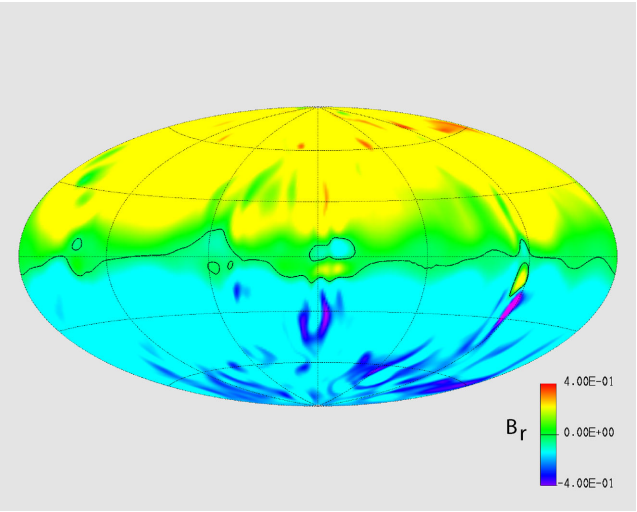

Figure 4. Snapshot of the radial magnetic field at the CMB from the geodynamo model. A strong dipole field is produced by the presence of a 360 km stratified layer at the top of the core.

and this feature is amplified by the presence of a thick stratified layer (see Fig. 4). On the other hand, our goal is to assess the interplay between a stratified layer and the underlying convection, so the details of the field morphology at the CMB is perhaps less important than the strength of the stratification.

Estimates for $\mathbf{V} \cdot \nabla c$ are extracted from the numerical solution over a range of spherical harmonic degrees. Each result is used to evaluate the corresponding source amplitude, $s_l(r, t)$. Taking the Fourier transform of $s_l(r, t)$ defines the forced response in (24). The largest response is expected when the frequency of $s_l(r, t)$ matches the frequency of the wave. Power spectra for $s_l(r, t)$ at the base of the stratified layer are shown in Fig. 5 for even ($l = 2, 4, 6$) and odd ($l = 1, 3, 5$) degrees. For reference, a vertical line is shown in Fig. 5 to mark the frequency of a nominal 60 yr oscillation. Even-degree spectra have nearly the same amplitude at the 60 yr period. Waves with $l = 2$ are predicted to have periods slightly longer than 60 yr (e.g. Buffett *et al.* 2016), whereas waves with $l = 6$ should have somewhat shorter periods. However, the overall level of excitation at periods close to the nominal value of 60 yr is similar among these three waves. Shorter wavelength waves ($l > 6$) have progressively higher natural frequencies and the overall level of excitation is predicted to be lower due to the decrease in the source terms at higher frequency. Consequently, it is reasonable on the basis of our numerical geodynamo model to expect zonal MAC waves to be predominantly low degree. Odd degrees have substantially lower source amplitudes. In particular, the excitation at $l = 1$ is roughly two orders of magnitude smaller than the even source terms at a nominal 60 yr period. While odd-degree waves should be present in the core, we can expect their amplitude to be smaller than the even-degree waves.

The geodynamo model predicts smaller contributions for the inertial and magnetic source terms. The rms value of the non-dimensional inertial force, $f_\phi = -(\mathbf{V} \cdot \nabla \mathbf{V})_\phi$, is approximately 1600 at the base of the stratified layer. (We consider the $l = 3$ component of the force because it contributes most to the $l = 2$ wave.) Integrating f_ϕ across the stratified layer gives $F_\phi = 220$. A similar value is obtained for the non-dimensional magnetic force, $f_\phi = (\mathbf{B} \cdot \nabla \mathbf{B})_\phi / EPm \approx 1800$; the integrated value is $F_\phi = 180$. The associated source terms from (30) and (32) can now be compared with the source term, S, due to buoyancy. The ratio of the inertial to buoyancy sources at degree l is

$$\frac{S_R}{S} \approx \frac{1}{2} \frac{F_\phi}{\langle s_l \rangle} E \, T'(R) \, l(l+1) \tag{34}$$

where $\langle s_l \rangle$ is the rms value of the temperature fluctuation, $T'(R) = 0.60$ is the radial temperature gradient at the CMB and l denotes the degree of the wave. The rms temperature fluctuation at $l = 2$ is $\langle s_2 \rangle$ =3.6, so the inertial source is about 0.9 per cent of the source due to buoyancy. Similarly, the magnetic source term is about 0.8 per cent of the buoyancy source. The relative importance of inertia is expected to decrease as the value of E decreases toward an Earth-like value. On the other hand, the relative importance of buoyancy and magnetic forces might be preserved if convection in the underlying region establishes a balance between buoyancy, magnetic and Coriolis forces (Yadav *et al.* 2016; Aubert *et al.* 2017). Waves with higher l would have comparatively larger contributions from the magnetic and inertial source terms.

More quantitative predictions for the effects of buoyancy forces are given by the wave amplitudes, c_k, which depend on the projection of the source amplitude $s_l(x)$ onto the eigenfunction for the wave $b_l^{(k)}(x)$ (see 26). Numerical estimates for $s_l(x)$ from the dynamo model occasionally extend across most of the stratified layer, but this outcome depends on the strength of the stratification. In the numerical dynamo model the convective temperature anomalies below the stratified layer are comparable in amplitude to the temperature change across the stratified layer (see Fig. 1). Thus thermal anomalies in the convecting region can rise through a large fraction of the stratified layer. In fact, we observe a local reversal in the

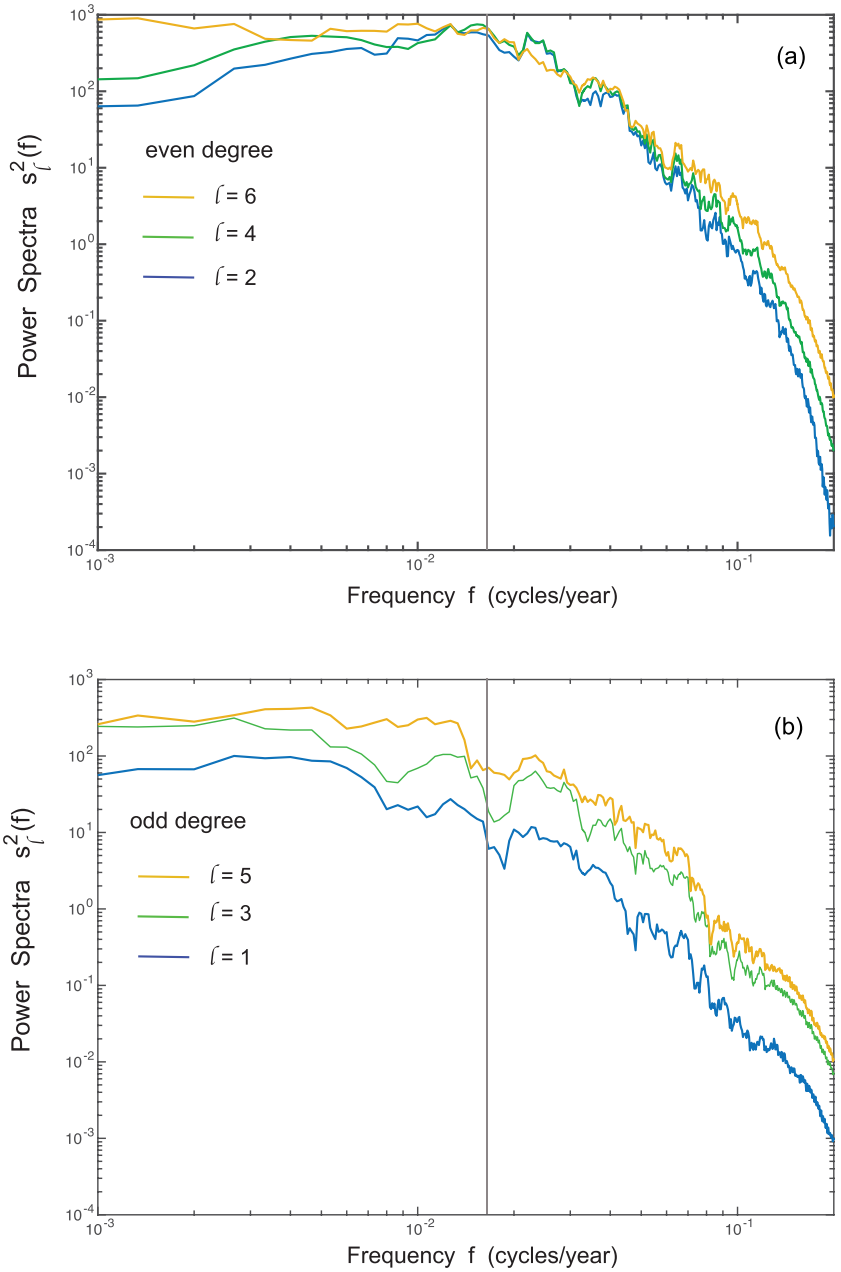

Figure 5. Power spectra of the source term for even (a) and odd (b) degrees. For reference, a vertical line defines the location of a 60 yr oscillation. These power spectra are relatively flat spectra at frequencies less than 10^{-2} cycles yr^{-1} or periods longer than 100 yr. The power drops off sharply once the period is shorter than 60 yr.

direction of CMB heat flow when warm parcels rise close to the CMB. Stronger stratification suppresses the penetration of thermal anomalies, so the source amplitude becomes much smaller near the top of the stratified layer. This means that the generation of wave motion, according to (26), is heavily weighted by the structure of the waves in the lower part of the layer. This is liable to be the situation in Earth's core if the stratification is roughly $N = 0.84\ \Omega$ (Buffett *et al.* 2016). Such a stratification would correspond to a temperature gradient (relative to the adiabat) of 0.037 K km^{-1}. Over a 140-km layer, we could accumulate a temperature anomaly of roughly 5.2 K, which is large compared to a typical convective anomaly of a few mK (Bloxham & Jackson 1990; Aurnou *et al.* 2003). (Compositional anomalies would yield an equivalent thermal anomaly based on the expected magnitude of c).

Fig. 6 shows the eigenfunctions $b_\phi^{(k)}$ for a pair of MAC waves from the numerical solution of Buffett *et al.* (2016), based on the model parameters $N = 0.84\ \Omega$ and $H = 140$ km. While these waves do not permit solutions by separation of variables due to the assumed form of the radial magnetic field, it is still possible to characterize the solutions by a dominant l. The fundamental and first overtone for the $l = 4$ wave reveal a distinct radial structure. The amplitude of $\mathbf{b}_\phi^{(k)}$ for the first overtone is larger in the lower part of the layer compared to that for the fundamental wave. This difference can enhance the generation of the first overtone when the source term is confined the lower part of the layer. This enhanced generation may partially compensate for the higher damping of the overtone, which would otherwise reduce the response to an imposed forcing. The prevalence of overtones among the waves needed to account for

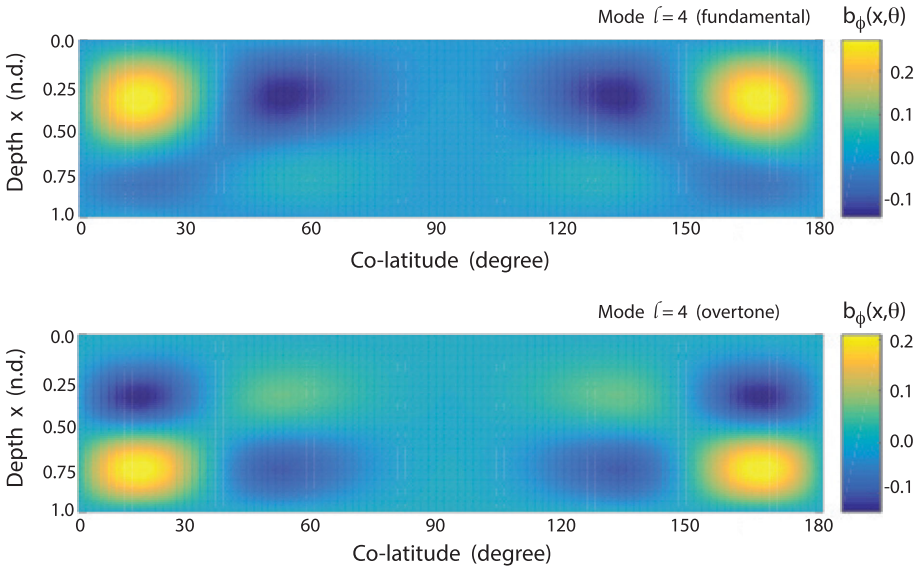

Figure 6. Eigenfunctions for the fundamental (a) and first overtone (b) of the $l = 4$ wave from the numerical calculation of Buffett *et al.* (2016). A larger amplitude in the lower part of the stratified layer means that the generation processes is more effective when the source term is confined to the lower part of the layer. The large amplitude for the first overtone could explain the prominence of overtones in the fit of MAC waves to core-surface flows.

models of core-surface flow (despite heavier damping) is compatible with the idea that zonal MAC waves are generated primarily near the base of the stratified layer.

7 DISCUSSION

Source amplitudes due to buoyancy in the geodynamo model can be characterized as brief events that occur at irregular intervals (see Fig. 3). The short duration of each event can be treated as nearly impulsive forces and the recurrence time is nominally 100–200 yr. Longer intervals are occasionally observed where there is no significant forcing. A complementary perspective of the recurrence interval comes from the power spectra in Fig. 5. A nearly flat spectra at low frequency is compatible with random, uncorrelated forcing at long periods. The corner frequency in the power spectra corresponds to a period of roughly 60 yr, so we might expect the time between large and independent excitations to be longer than 60 yr. Once the MAC waves are generated by an impulsive source their amplitudes gradually decay with time. A typical decay time for waves from the study of Buffett *et al.* (2016) was 100 yr or less. (The longest decay time corresponds to the lowest l.) This suggests that waves can undergo substantial decay between typical source events. Thus the relative amplitude of the various waves could be highly variable in time. The fact that we currently observe a dominant 60 yr period might reflect only the present transient state in the core. Future sources of excitation could produce very different combinations of waves. Consequently, the dominant period at some time in the future might be quite different than 60 yr. For example, a dominant $l = 2$ wave would correspond to a 116 yr period, according to the predictions in Buffett *et al.* (2016). Periods shorter than 60 yr are also possible.

Insights into the underlying convection can be extracted from more detailed investigations of the generation process. For example, we might convolve the Green's function with a finite duration source to estimate how quickly the amplitudes and phases of the various waves change. These predictions could be compared with the amplitude and phase of MAC waves needed to account for core-surface flow or dipole fluctuations over longer intervals of time. Such comparisons would furnish information about the duration of the source, which could be related to the size and velocity of buoyant parcels in the core. Achieving this goal would require a more general description of the Green's function to allow more flexible descriptions of the density stratification and the distribution of radial magnetic field, but in principle we can construct a physical model that connects observable waves to the processes that generate them. Current estimates of zonal core-surface flow are mostly (or entirely) symmetric about the equator, which supports the notion that the source function is largest for even degrees. This expectation is consistent with the nature of rapidly rotating flow (Jones 2011; Jault & Finlay 2015), and it is compatible with the predictions of a geodynamo model.

8 CONCLUSIONS

Convection in Earth's core is an effective mechanism for generating MAC waves in a stratified layer below the CMB. We describe a method for quantifying the generation of axisymmetric MAC waves and illustrate the approach using a simple, analytical model (Braginsky 1993). However, the general approach can be extended to permit more realistic wave models. Numerical estimates for the source terms are obtained from a geodynamo model. We find that the largest source terms are due to buoyancy forces, and most of the excitation occurs at even spherical harmonic degrees, corresponding to waves with azimuthal flow that is symmetric about the equator. Power spectra for the source terms suggest that the amplitude of wave generation decreases at periods shorter than about 60 yr. This result implies that most of the wave generation is confined to low-degree waves, although the relative amplitude of these waves is liable to change over time.

Quantitative estimates for the wave amplitudes depend on the projection of the source term onto the eigenfunctions of the individual waves. Strong stratification due to either thermal (Gubbins *et al.* 1982; Lister & Buffett 1998) or compositional effects (Buffett & Seagle 2010; Gubbins & Davies 2013) limits the penetration of convective density anomalies into the stratified layer. As a result the source terms are restricted to the lowermost part of the

layer. Overtones with large wave amplitudes in the lower part of the stratified layer are more effectively generated by convection even though these waves are heavily damped by magnetic diffusion. This behaviour may explain the prominence of overtones when MAC waves are fit to models of core-surface flow.

Generation of MAC waves by convection in the core provides a physical link between observable wave motion at the surface of the core and the deeper convective processes. Detection of changes in the amplitude and phase of MAC waves would constrain the generation process and potentially offer new insights into the nature of convection.

ACKNOWLEDGEMENTS

This work is partially supported by an ENS student internship to EJ from the University of Lyon and by a grant from the National Science Foundation (EAR-1430526) to BB. We thank Hiro Matsui for assistance with *Calypso* and two anonymous reviewers for constructive comments and suggestions.

REFERENCES

Aubert, J., Gastine, T. & Fournier, A., 2017. Spherical convective dynamos in the rapidly rotating asymptotic regime, *J. Fluid Mech.,* **813**, 558–593.

Aurnou, J.M., Andreadis, Zhu L. & Olson, P., 2003. Experiments on convection in Earth's core tangent cylinder, *Earth planet. Sci. Lett.,* **212,** 119–134.

Aurnou, J.M., Calkins, M.A., Cheng, J.S., Julien, K., King, E.M., Nieves, D., Soderlund, K.M. & Stellmach, S., 2015. Rotating convective turbulence in Earth and planetary cores, *Phys. Earth planet. Inter.,* **246,** 52–71.

Braginsky, S.I., 1984. Short-period geomagnetic secular variation, *Geophys. Astrophys. Fluid Dyn.,* **30,** 1–78.

Braginsky, S.I., 1993. MAC-oscillations of the hidden ocean of the core, *J. Geomag. Geoelectr.,* **45,** 1517–1538.

Bloxham, J. & Jackson, A., 1990. Lateral temperature variations at the core-mantle boundary deduced from the magnetic field, *Geophys. Res. Lett.,* **17,** 1997–2000.

Buffett, B., 2014. Geomagnetic fluctuations reveal stable stratification at the top of the Earth's core, *Nature,* **507,** 484–487.

Buffett, B.A. & Seagle, C.T., 2010. Stratification of the top of the core due to chemical interactions with the mantle, *J. geophys. Res.,* **115,** B04407, doi:10.29/2009JB006751.

Buffett, B., Knezek, N. & Holme, R., 2016. Evidence for MAC waves at the top of Earth's core and implications for variations in length of day, *Geophys. J. Int.,* **204,** 1789–1800.

Christensen, U.R., Aubert, J. & Hulot, G., 2010. Conditions for Earth-like geodynamo models, *Earth planet. Sci. Lett.,* **296,** 487–496.

Dahlen, F.A. & Tromp, J., 1998. *Theoretical Global Seismology,* Princeton Univ. Press.

Gillet, N., Jault, D., Finlay, C.C. & Olsen, N., 2013. Stochastic modeling of the Earth's magnetic field: inversion for covariances over the observatory era, *Geochem. Geophys. Geosys.,* **14,** 766–786.

Gillet, N., Jault, D. & Finlay, C.C., 2015. Planetary gyre, time-dependent eddies, torsional waves, and equatorial jets at the Earth's core surface, *J. geophys. Res.,* **120,** 3991–4013.

Goldreich, P. & Kumar, P., 1990. Wave generation by turbulent convection, *Astrophys. J.,* **363,** 694–704.

Gubbins, D. & Roberts, P.H., 1987. Magnetohydrodynamics of the Earth's Core, in *Geomagnetism,* vol. 2, pp. 1–184, ed. Jacobs, J.A., Academic Press.

Gubbins, D. & Davies, C.J., 2013. The stratified layer at the core-mantle boundary caused by barodiffusion of oxygen, sulphur and silicon, *Phys. Earth planet. Inter.,* **215,** 21–28.

Gubbins, D., Thompson, C.J. & Whaler, K.A., 1982. Stable regions in the Earth's liquid core, *Geophys. J. R. astr. Soc.,* **68,** 241–251.

Holme, R., 2015. Large-scale flow in the core, in *Treatise on Geophysics,* 2nd ed., vol. 8, pp. 91–113, ed. Schubert, G., Elsevier.

Hori, K., Jones, C.A. & Teed, R.J., 2015. Slow magnetic Rossby waves in the Earth's core, *Geophys. Res. Lett.,* **42,** 6622–6629.

Houdek, G., Balmforth, N.J., Christensen-Dalsgaard, J. & Gough, D.O., 1999. Amplitude of stochastically excited oscillations in main-sequence stars, *Astron. Astrophys.,* **351,** 582–596.

Hulot, G. & Le Mouel, J.-L., 1994. A statistical approach to the Earth's main magnetic field, *Phys. Earth planet. Inter.,* **82,** 167–183.

Jackson, A., 1997. Time-dependency of tangentially geostrophic core surface motions, *Phys. Earth planet. Inter.,* **103,** 293–311.

Jackson, A., Jonkers, A.R.T. & Walker, M.R., 2000. Four centuries of geomagnetic secular variation from historical records, *Phil. Trans. R. Soc. A,* **358,** 957–990.

Jault, D. & Finlay, C.C., 2015. Waves in the core and mechanical core-mantle interactions, in *Treatise on Geophysics,* 2nd ed., vol. 8, pp. 225–244, ed. Schubert, G., Elsevier.

Jones, C.A., 2011. Planetary magnetic fields and fluid dynamos, *Annu. Rev. Fluid Mech.,* **43,** 583–614.

Lecoanet, D. & Quataert, E., 2012. Internal gravity wave excitation by turbulent convection, *Mon. Not. R. astr. Soc.,* **430,** 2363–2376.

Lecoanet, D., Le Bars, M., Burns, K.J., Vasil, G.M., Brown, B.P., Quataert, E. & Oishi, J.S., 2015. Numerical simulations of internal wave generation by convection in water, *Phys. Rev. E,* **91,** 063016, doi:10.1103/PhysRevE.91.063016.

Lhuillier, F., Fournier, A., Hulot, G. & Aubert, J., 2011. The geomagnetic secular-variation timescale in observations and numerical dynamo models, *Geophys. Res. Lett.,* **38,** L09306, doi:10.1029/2011GL047356.

Lighthill, M.J., 1952. On sound generation aerodynamically. I. General Theory, *Proc. R. Soc. A,* **211,** 564–587.

Lister, J.R. & Buffett, B.A., 1998. Stratification of the outer core at the core-mantle boundary, *Phys. Earth planet. Inter.,* **105,** 5–19.

Lognonné, P., 1991. Normal modes and seismograms in an anelastic rotating Earth, *J. geophys. Res.,* **96,** 20 309–20 319.

Matsui, H., King, E. & Buffett, B., 2014. Multiscale convection in a geodynamo simulation with uniform heat flux along the outer boundary, *Geochem. Geophys. Geosyst.,* **15,** 3212–3225.

Olson, P., Deguen, R., Rudolph, M.L. & Zhong, S.J., 2015. Core evolution driven by mantle global circulation, *Phys. Earth planet. Inter.,* **243,** 44–55.

Pandya, R.E. & Alexander, M.J., 1999. Linear stratospheric gravity waves above convective thermal forcing, *J. Atmos. Sci.,* **56,** 2434–2446.

Pedlosky, J., 1987. *Geophysical Fluid Dynamics,* 2nd edn, Springer-Verlag, 715 pp.

Phillips, O.M., 1966. *The Dynamics of the Upper Ocean,* Cambridge Univ. Press, 261 pp.

Press, W.H., 1981. Radiative and other effects from internal waves in solar and stellar interiors, *Astrophys. J.,* **245,** 286–303.

Stein, R.F., 1967. Generation of acoustic and gravity waves by turbulence in an isothermal stratified atmosphere, *Sol. Phys.,* **2,** 385–432.

Teed, R.J., Jones, C.A. & Tobias, S.M., 2014. The dynamics and excitation of torsional waves in geodynamo simulations, *Geophys. J. Int.,* **196,** 724–735.

Teed, R.J., Jones, C.A. & Tobias, S.M., 2015. The transition to Earth-like torsional oscillations in magnetoconvection simulations, *Earth planet. Sci. Lett.,* **419,** 22–31.

Wardinski, I. & Lesur, V., 2012. An extended version of the C^3FM geomagnetic field model: application of a continuous frozen-flux constraint, *Geophys. J. Int.,* **189,** 1409–1429.

Yadav, R.K., Gastine, T., Christensen, U.R., Wolk, S.J. & Poppenhaeger, K., 2016. Approaching a realistic force balance in geodynamo simulations, *Proc. Natl. Acad. Sci. USA,* **113,** 12 065–12 070.

APPENDIX A: WAVE EQUATION FOR ZONAL MAC WAVES

Braginsky (1993) converts the governing eqs (1)–(3) into a single scalar wave equations for b_ϕ. We follow his treatment but include

an additional term to describe the change in the buoyancy force due to the influence of background convection. This additional term defines an excitation source in the wave equation. When the effects of inertia and viscous forces are omitted from the momentum equation, the leading-order terms in the MAC force balance are

$$g\,c = -\frac{1}{\rho}\frac{\partial P}{\partial r} \tag{A1}$$

$$2\Omega_r v_\phi = \frac{1}{\rho r}\frac{\partial P}{\partial \theta} \tag{A2}$$

$$2\Omega_r v_\theta = \frac{B_r}{\rho\mu}\frac{\partial b_\phi}{\partial r} \tag{A3}$$

where B_r and Ω_r are the radial components of the background magnetic field and rotation vector. Magnetic perturbations in the θ and ϕ directions are governed by

$$\frac{\partial b_{\theta,\phi}}{\partial t} - \eta\frac{\partial^2 b_{\theta,\phi}}{\partial r^2} = B_r\frac{\partial v_{\theta,\phi}}{\partial r} \tag{A4}$$

whereas the radial component b_r can be computed from the solenoidal condition $\nabla \cdot \mathbf{b} = 0$. Similarly, the radial component of the velocity field in a thin layer is given by

$$\frac{\partial v_r}{\partial r} = -\frac{1}{R\sin\theta}\frac{\partial(\sin\theta\, v_\theta)}{\partial\theta} \tag{A5}$$

where R is the radius of the CMB. Substituting for v_θ from (A3) and integrating over radius yields

$$v_r = -\left(\frac{B_r}{2\Omega_r\rho\mu R}\right)\frac{1}{\sin\theta}\frac{\partial(\sin\theta b_\phi)}{\partial\theta} \tag{A6}$$

where we use the boundary condition $v_r = b_\phi = 0$ at $r = R$ to evaluate the integration constant.

Eliminating pressure P from (A1) and (A2) relates the azimuthal flow v_ϕ to the buoyancy force $g\,c$. Substituting for v_ϕ in the ϕ component of the induction in (A4) gives

$$\frac{\partial b_\phi}{\partial t} - \eta\frac{\partial^2 b_\phi}{\partial r^2} = -\left(\frac{B_r}{2\Omega_r R}\right)\frac{\partial(g\,c)}{\partial\theta} \tag{A7}$$

where we can reasonably approximate g as a constant. Taking the time derivative of (A7) and substituting for the evolution of the buoyancy force from (5) gives

$$\frac{\partial^2 b_\phi}{\partial t^2} - \eta\frac{\partial^3 b_\phi}{\partial r^2\partial t} = -\left(\frac{B_r}{2\Omega_r R}\right)\frac{\partial}{\partial\theta}(N^2 v_r - g\mathbf{V}\cdot\nabla c) \tag{A8}$$

Finally, we substitute for v_r from (A6) to obtain

$$\frac{\partial^2 b_\phi}{\partial t^2} - \eta\frac{\partial^3 b_\phi}{\partial r^2\partial t} - \left(\frac{B_r^2 N^2}{4\Omega_r^2 R^2\rho\mu}\right)\mathcal{L}_\theta^2 b_\phi = S \tag{A9}$$

where the source S is defined in (8) and the operator $\mathcal{L}_\theta^2$ is defined in (9).

APPENDIX B: ORTHOGONALITY CONDITION FOR MAC WAVES

A Green's function for the impulse response can be constructed from the eigenfunctions of the unforced problem. We begin with the Fourier transform of the wave equation from (15). Solutions for the unforced motion have frequencies ω_k and eigenfunctions $\tilde{b}_l^{(k)}$. When we adopt the stretched coordinate $x = (R - r)/H$, the solutions obey the wave equation

$$-\omega_k^2\tilde{b}_l^{(k)} + i\left(\frac{\omega_k\eta}{H^2}\right)\partial_x^2\tilde{b}_l^{(k)} + \omega_l^2\tilde{b}_l^{(k)} = 0\,. \tag{B1}$$

where ω_l^2 characterizes the restoring force for the waves. Multiplying (B1) by a second eigenfunction, $\tilde{b}_l^{(j)}$, and integrating over the domain gives

$$(\omega_l^2 - \omega_k^2)\int_0^{1^+}\tilde{b}_l^{(j)}\tilde{b}_l^{(k)}\,\mathrm{d}x + i\left(\frac{\omega_k\eta}{H^2}\right)\int_0^{1^+}\tilde{b}_l^{(j)}\partial_x^2\tilde{b}_l^{(k)}\,\mathrm{d}x = 0 \tag{B2}$$

where $x = 1^+$ defines the depth at which the eigenfunction vanishes inside the core. We integrate the second term in (B2) by parts, and use the boundary condition $\tilde{b}_l = 0$ at $x = 0$ and $x = 1^+$, to obtain

$$(\omega_l^2 - \omega_k^2)[\tilde{b}_l^{(j)}, \tilde{b}_l^{(k)}] - i\frac{\omega_k\eta}{H^2}[\partial_x\tilde{b}_l^{(j)}, \partial_x\tilde{b}_l^{(k)}] = 0 \tag{B3}$$

where we introduce the notation Lognonné (1991)

$$[a, b] = \int_0^{1^+}(a\,b)\,\mathrm{d}x\,. \tag{B4}$$

Interchanging indices j and k and taking the difference from (B3) gives

$$(\omega_j^2 - \omega_k^2)[\tilde{b}_l^{(j)}, \tilde{b}_l^{(k)}] + i\frac{\eta}{H^2}(\omega_j - \omega_k)[\partial_x\tilde{b}_l^{(j)}, \partial_x\tilde{b}_l^{(k)}] = 0\,. \tag{B5}$$

Factoring $\omega_j^2 - \omega_k^2$ and dividing (B5) by $\omega_j - \omega_k$ yields the orthogonality condition

$$(\omega_j + \omega_k)[\tilde{b}_l^{(j)}, \tilde{b}_l^{(k)}] + i\frac{\eta}{H^2}[\partial_x\tilde{b}_l^{(j)}, \partial_x\tilde{b}_l^{(k)}] = 0\,. \tag{B6}$$

We can define a normalization for the eigenfunctions by setting $j = k$ and letting $\omega_j \to \omega_k$. Thus we obtain

$$2\omega_k[\tilde{b}_l^{(k)}, \tilde{b}_l^{(k)}] + i\frac{\eta}{H^2}[\partial_x\tilde{b}_l^{(k)}, \partial_x\tilde{b}_l^{(k)}] = 1\,. \tag{B7}$$

We now use the orthogonality condition to obtain a solution to the forced problem. When the source term is impulsive (i.e. $s_l(x, t) = s_l(x)\delta(t)$), the Fourier transform of the wave equation from (24) can be written as

$$-\omega^2\tilde{b}_l(x, w) + i\frac{\omega\eta}{H^2}\partial_x^2\tilde{b}_l(x, \omega) + \omega_l^2\tilde{b}_l(x, \omega) = -\left(\frac{g B_d}{2\Omega R}\right)s_l(x) \tag{B8}$$

After the application of an impulse force, the motion can be represented by a linear combination of waves (as shown in 25). Taking the Fourier transform of (25) gives

$$\tilde{b}_l(x, \omega) = \sum_k\frac{i c_k}{\omega - \omega_k}\tilde{b}_l^{(k)}\,. \tag{B9}$$

We now substitute (B9) into (B8) to define a condition on the constants c_k. If we multiply this condition by $\tilde{b}_l^{(j)}$ and integrate over x, we obtain

$$\sum_k\frac{i c_k}{\omega - \omega_k}\left((\omega_l^2 - \omega^2)[\tilde{b}_l^{(j)}, \tilde{b}_l^{(k)}] - i\frac{\omega\eta}{H^2}[\partial_x\tilde{b}_l^{(j)}, \partial_x\tilde{b}_l^{(k)}]\right) = -\left(\frac{g B_d}{2\Omega R}\right)\int_0^{1^+}\tilde{b}_l^{(j)}s_l\,\mathrm{d}x\,. \tag{B10}$$

To extract numerical values for the constants, c_k, we note that

$$\sum_k\frac{i c_k}{\omega - \omega_k}\left((\omega_l^2 - \omega_k^2)[\tilde{b}_l^{(j)}, \tilde{b}_l^{(k)}] - i\frac{\omega_k\eta}{H^2}[\partial_x\tilde{b}_l^{(j)}, \partial_x\tilde{b}_l^{(k)}]\right) = 0 \tag{B11}$$

by virtue of (B3), so we take the difference between (B10) and (B11) to obtain

$$\sum_k i c_k \left((\omega + \omega_k)[\tilde{b}_l^{(j)}, \tilde{b}_l^{(k)}] + i \frac{\eta}{H^2} [\partial_x \tilde{b}_l^{(j)}, \partial_x \tilde{b}_l^{(k)}] \right) = \left(\frac{g B_d}{2\Omega R} \right) \int_0^{1^+} \tilde{b}_l^{(j)} s_l \, \mathrm{d}x \tag{B12}$$

Finally, we let $\omega \to \omega_j$, so that each term in the summation over k vanishes unless $j = k$. From the single surviving term we find

$$c_j = -i \left(\frac{g B_d}{2\Omega R} \right) \int_0^{1^+} \tilde{b}_l^{(j)} s_l(x) \, \mathrm{d}x \, . \tag{B13}$$